

Reconfigurable MDI-QKD and BB84 over 20 km optical channels via EOM-tailored weak coherent states

Jaesung Lim, Yonggi Jo, Nam Hun Park, Zaeill Kim, and Yong Sup Ihn*
Agency for Defense Development, Daejeon 34186, Korea
 (Dated: June 10, 2026)

Measurement-device-independent quantum key distribution (MDI-QKD) is designed to eliminate detector side-channel vulnerabilities. However, its practical deployment remains experimentally demanding because it requires two-photon interference (TPI) between mutually phase-randomized optical states. In this study, we demonstrate a reconfigurable platform that supports both polarization-encoded MDI-QKD and BB84 measurements utilizing the same optical hardware over 20 km optical fiber channels. Two mutually phase-randomized weak coherent states (WCSs) are generated from a shared continuous-wave (CW) laser via electro-optic phase modulation and subsequent etalon-based first-order sideband filtering. Channel indistinguishability is verified through Hong–Ou–Mandel (HOM) interference, combining time-resolved coincidence measurements and polarization mismatch scans, confirming a high degree of indistinguishability that robustly approaches the classical upper limit of 0.5 for WCSs. The transmitted states go through partial Bell-state measurement (BSM) to implement MDI-QKD. Here, the system can be directly reconfigured for BB84 simply by rotating a single half-wave plate (HWP) by 22.5° in one arm of the module. This seamless reconfiguration drastically reduces hardware redundancy and enhances operational flexibility in dynamic network environments. These results indicate that EOM-based frequency engineering using a shared CW laser offers a highly practical route toward scalable and reconfigurable quantum communication systems.

I. INTRODUCTION

When two indistinguishable photons impinge on a beam splitter, bosonic bunching suppresses coincident detection at the two output ports. This phenomenon, known as the Hong–Ou–Mandel (HOM) dip, arises when two input photons are perfectly matched in all relevant degrees of freedom, including polarization, spectrum, spatial mode, and arrival time [1]. Consequently, it has become the standard benchmark for verifying photon indistinguishability [2]. While initially demonstrated with nonclassical biphoton states from spontaneous parametric down-conversion (SPDC), HOM interference can also be realized using phase-randomized weak coherent states (WCSs) [3–9]. Although the Poissonian photon-number statistics of WCSs impose a theoretical visibility upper bound of 50%, the technological maturity of coherent sources makes WCS-based two-photon interference (TPI) a practical building block for quantum information protocols [10].

A prominent application of this fundamental building block is measurement-device-independent quantum key distribution (MDI-QKD) [11]. While theoretical QKD guarantees unconditional security based on quantum mechanics, real-world physical device imperfections can expose critical side-channel vulnerabilities [12, 13]. Although device-independent QKD solves this fundamentally, it demands near-unity detection efficiencies that remain challenging for practical deployment [14]. In contrast, MDI-QKD circumvents all detector side channels while maintaining compatibility with realistic experimental constraints [15–18]. However, MDI-QKD generally

yields lower key generation rates compared to conventional decoy-state BB84 protocols because it relies on two-photon coincidences.

This intrinsic trade-off highlights the necessity for reconfigurable QKD platforms capable of dynamically switching between MDI-QKD and decoy-state BB84 based on the level of trust assigned to intermediate network nodes [19, 20]. In this work, we implement an electro-optic modulator (EOM)-based reconfigurable QKD platform. EOMs provide high optical transmission efficiency alongside precise frequency control [21]. By splitting the output of a single CW laser and driving phase modulation with independent radio frequency (RF) signals, we successfully produce two mutually phase-randomized WCS channels. We thoroughly characterize the two-photon indistinguishability using time-resolved TPI and polarization-mismatch scans, and demonstrate polarization-encoded MDI-QKD and BB84 operations, measuring the corresponding quantum bit error rates (QBERs).

II. EXPERIMENTAL SETUP

The schematic of the reconfigurable quantum cryptographic platform is illustrated in Fig. 1(a). A tunable distributed feedback (DFB) laser operating near 1550 nm serves as the common CW light source. The laser output is split via a 50:50 beam splitter (BS) to form independent transmitter channels for Alice and Bob. In each channel, a polarization controller (PC) and a polarizing beam splitter (PBS) are positioned to optimize the input polarization and precisely adjust the optical intensity before entering the EOM. The EOMs are driven by independent 9.5 GHz RF sources.

* yong0862@add.re.kr

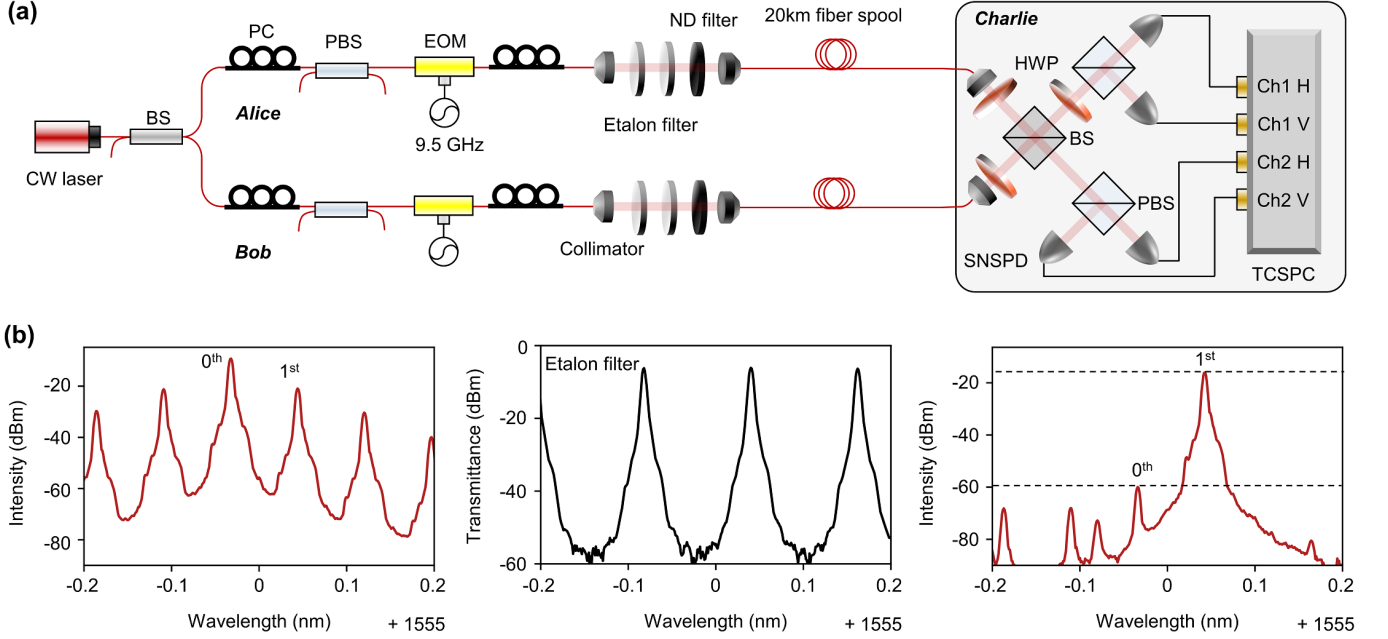


FIG. 1. Experimental setup and spectral characterization of the reconfigurable QKD platform. (a) Schematic of the optical architecture. Two mutually phase-randomized weak coherent states (WCSs) are generated from a single CW laser using EOMs driven by independent 9.5 GHz RF sources, followed by sideband filtering. After propagating through a 20 km optical fiber spool, the signals enter Charlie’s partial Bell-state measurement module. The system is reconfigured between MDI-QKD and BB84 modes simply by toggling a specific HWP in channel 1 to either 0° or 22.5° . (b) The spectra of the WCS preparation. The leftmost panel shows the raw optical spectrum after EOM phase modulation. The middle panel displays the transmission profile of two cascaded etalon filters. The rightmost panel confirms the isolation of the first-order sideband, demonstrating a residual carriers suppression of approximately 40 dB.

The spectral engineering process is characterized in Fig. 1(b). As shown in the left spectral data of Fig. 1(b), the raw output from the EOM exhibits a series of sidebands generated at intervals of 9.5 GHz centered around the carrier frequency (0th order). To isolate a single sideband (1st order), the modulated light is passed through two cascaded etalon filters. These etalons feature a free spectral range (FSR) of approximately 15 GHz and an extinction ratio close to 50 dB, as detailed in the middle panel of Fig. 1(b). The resulting filtered spectrum, shown in the right panel, proves that the selected first-order sideband suppresses the residual carrier by approximately 40 dB, confirming prominent sideband isolation. Due to the DFB laser’s tunability, adjusting the center wavelength allows the first-order sideband to align with etalon transmission peaks, enabling the generation of WCS channels across different wavelength bins without physical hardware modifications.

Following sideband generation, Alice and Bob encode polarization states ($|H\rangle$, $|V\rangle$ for the Z basis; $|D\rangle$, $|A\rangle$ for the X basis) using PCs and half wave plates (HWPs), sending their signals through a 20 km fiber spool to the untrusted relay node, Charlie. The optical signals are attenuated to the single-photon level via neutral density (ND) filters. Charlie’s measurement setup features a partial BSM module capable of identifying the $|\psi^+\rangle$ and $|\psi^-\rangle$ Bell states. Incoming photons are detected by four superconducting nanowire single-photon detectors

(SNSPDs) and processed via a time-correlated single-photon counter (TCSPC) with a 10 ns coincidence window.

To reconfigure the system between MDI-QKD and BB84 protocols, a single HWP is located in the one arm of Charlie’s partial BSM module as depicted in Fig. 1(a). When this HWP is set to 0° , the hardware functions as a standard MDI-QKD receiver. Rotating this HWP to 22.5° converts the Z-basis measurement in that arm into an X-basis projection. This architectural shift enables Charlie to simultaneously project incoming single-photon states onto both bases, effectively implementing the BB84 measurement framework using the same physical hardware [19, 20]. Furthermore, to prevent potential side-channel attacks or detector malfunctions during the operational transition between MDI-QKD and BB84, it is necessary to physically isolate the communication link. Specifically, when executing the BB84 protocol over either the Alice-Charlie or Bob-Charlie link, the unused channel must be effectively blocked. In our current implementation, this is straightforwardly achieved by physically obstructing the inactive beam path with a mechanism such as a beam block. This simple yet highly effective security measure ensures robust protection without compromising the inherent convenience and cost-efficiency of our reconfigurable architecture, which dynamically adapts to network security demands using a single, unified hardware platform.

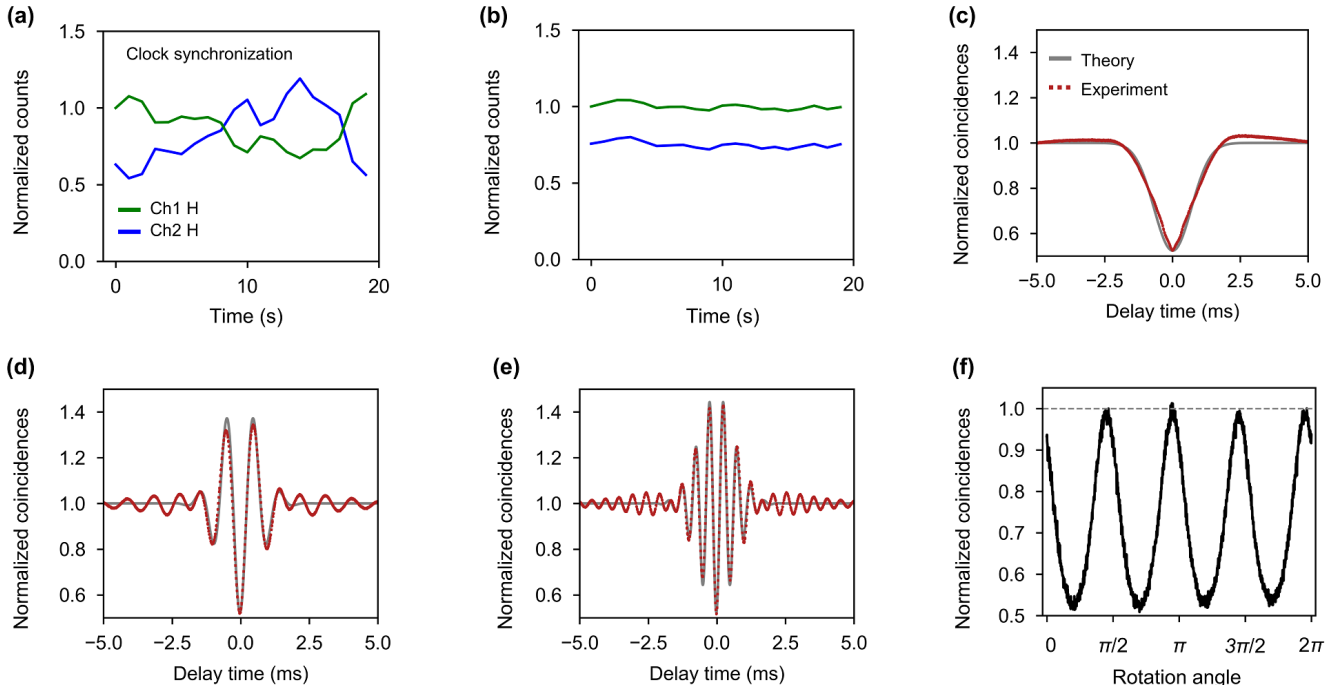


FIG. 2. Experimental verification of phase randomization and two-photon indistinguishability. (a,b) First-order interference traces recorded at the H-polarized outputs without the 20 km fiber spool, obtained with (a) synchronized and (b) independent RF source clocks. (c–e) Time-resolved Hong-Ou-Mandel (HOM) coincidence histograms as a function of the detection time difference Δt for frequency detunings of (c) 0 kHz, (d) 1 kHz, and (e) 2 kHz in Alice’s arm. The experimental data (red points) are well described by the theoretical fits (solid gray curves) based on Eq. (1). (f) A polarization mismatch scan demonstrating a four-period coincidence oscillation. The upper and lower bounds (gray dashed lines) are consistent with the HOM visibility limit.

III. RESULTS AND DISCUSSION

Prior to evaluating two-photon interference, it is critical to verify the mutual phase randomization of the two prepared WCS channels. We analyzed the first-order interference patterns at the H-polarized outputs of channels 1 and 2 without inserting the 20 km fiber spool. Photon count traces were measured for 20 s using a binwidth of 1 s. Figure 2(a) illustrates the trace obtained when the RF generator clocks are externally synchronized. In this configuration, the relative phase between the sidebands drift slowly, resulting in clear first-order interference oscillation over time. In contrast, as depicted in Fig. 2(b), when the RF generators operate on independent internal clocks, the complete absence of first-order interference patterns demonstrates that the mutual phase is fully randomized. This validates that the two channels function as phase-incoherent sources, satisfying a core operational prerequisite for secure MDI-QKD.

Because the mutual coherence time of these CW WCSs is significantly longer than any practical optical path delay, typical spatial scanning cannot characterize photon indistinguishability. Instead, we performed time-resolved TPI by recording coincidences as a function of the detection time difference Δt between the two output ports [6, 9]. When polarizations and intensities are

matched, the normalized coincidence rate is described by

$$g^{(2)}(\Delta t) = 1 - V \cos(\Delta\omega \Delta t) \exp\left(-\frac{\Delta t^2}{T_c^2}\right), \quad (1)$$

where V represents the visibility, $\Delta\omega$ is the angular frequency difference between the two channels, and T_c is the mutual coherence time.

Coincidence histograms were acquired with 1 μ s time bins over a 10 ms temporal window and accumulated for 1 min for each detuning setting. Figures 2(c), 2(d), and 2(e) show these time-resolved TPI measurements corresponding to frequency detunings of 0, 1, and 2 kHz, respectively. For zero frequency detuning (Fig. 2(c)), the minimum normalized coincidence level reaches 0.524, which corresponds to a visibility of $V = 0.476$, approaching the classical limit of 0.5 for WCSs. Fitting Eq. (1) to the data yields an average mutual coherence time of $T_c = 0.958$ ms. This value represents an effective mutual coherence time determined primarily by the phase noise of the independent RF generators and the phase fluctuations accumulated within the 20 km fiber spool.

To further validate channel indistinguishability, we conducted a polarization mismatch scan. With both channels initially prepared in the $|H\rangle$ state, an HWP in Alice’s arm was continuously rotated. As the angle θ is swept from 0 to 2π , the polarization returns to $|H\rangle$ four times. Figure 2(f) shows the corresponding coin-

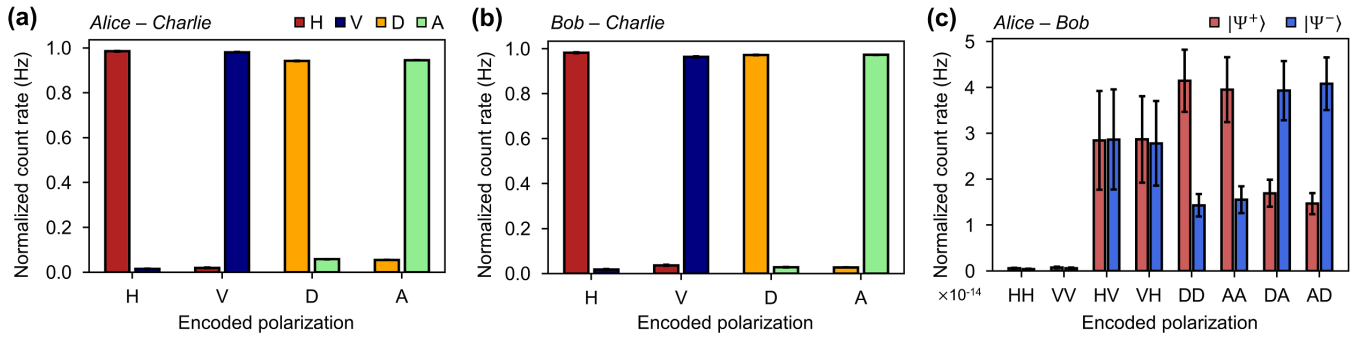


FIG. 3. Evaluation of QKD performance in the MDI-QKD and BB84 operation modes. (a,b) Normalized single-photon count rates measured in the BB84 mode, achieved by setting the internal HWP to 22.5° , for the (a) Alice–Charlie and (b) Bob–Charlie links. The bars indicate the detection probabilities across the four polarization states (H, V, D, A) for each encoded input. (c) Normalized coincidence count rates for the $|\psi^+\rangle$ and $|\psi^-\rangle$ Bell-state projections in the MDI-QKD mode (HWP at 0°). The data represent all 16 polarization combinations encoded between Alice and Bob, demonstrating distinct projection characteristics in the Z and X bases. All data points in both operational modes were accumulated over a 5 min measurement window.

cidence counts. The expected four-period oscillation is clearly observed, with maximum and minimum boundaries corresponding to the 0.476 visibility obtained from the time-resolved TPI.

We evaluated the system’s operational viability by measuring the QBERs for both MDI and BB84 configurations. For the BB84 mode (HWP set to 22.5°), data for each encoded polarization state were accumulated over 5 min. In this setup, the QBER is evaluated as:

$$E = \frac{C_\perp}{C_\parallel + C_\perp}, \quad (2)$$

where C_\parallel is the count rate of the detector associated with the successfully encoded polarization state, and C_\perp is the count rate of the orthogonal state within the same basis.

Figures 3(a) and 3(b) present these normalized single-photon count rates. For the Alice–Charlie link, the measured QBERs are $E_Z = (1.68 \pm 0.12)\%$ and $E_X = (5.62 \pm 0.05)\%$. For the Bob–Charlie link, they are $E_Z = (2.25 \pm 0.25)\%$ and $E_X = (2.75 \pm 0.06)\%$. The slight elevation of E_X in the Alice–Charlie link is due to minor beam splitter birefringence, which introduces different phase shifts to the H and V components upon reflection and transmission and thereby converts the nominally linear polarization into a slightly elliptical state. All measured BB84 QBERs remain comfortably below the 11% asymptotic security threshold.

Returning the internal HWP to 0° engages the MDI-QKD operation mode. Here, data for each encoded polarization state combination were again accumulated over 5 min. The measured coincidence counts are normalized by the square of the sum of all detector count rates. For the MDI-QKD measurements, we denote C_{ij}^\pm as the coincidence count for the $|\psi^\pm\rangle$ outcome when Alice and Bob encode states i and j , respectively, such that total coincidences are $C_{ij} = C_{ij}^+ + C_{ij}^-$. Based on these definitions, the QBERs for the Z and X bases, E_Z and E_X ,

are defined as

$$E_Z = \frac{C_{HH} + C_{VV}}{C_{HH} + C_{VV} + C_{HV} + C_{VH}}, \quad (3)$$

and

$$E_X = \frac{C_{DD}^- + C_{AA}^- + C_{DA}^+ + C_{AD}^+}{C_{DD}^- + C_{AA}^- + C_{DA}^+ + C_{AD}^+}. \quad (4)$$

Figure 3(c) shows the resulting normalized coincidence count rates evaluated via these metrics. We obtained experimental MDI-QKD QBERs of $E_Z = (2.1 \pm 0.7)\%$ and $E_X = (27.6 \pm 0.5)\%$ between Alice and Bob. These results demonstrate reasonable agreement with the corresponding theoretical expectations of 0% and 25%, respectively, confirming the robust cryptographic stability of the platform.

IV. CONCLUSION

We have demonstrated a highly versatile and reconfigurable QKD platform over a 20 km optical fiber channel. By employing EOM-driven sideband engineering, two mutually phase-randomized WCS channels were effectively prepared using a common CW laser source. This setup allows for a smooth transition between polarization-encoded MDI-QKD and BB84 modes simply by toggling a single HWP within the partial BSM module, leaving the remaining optical framework untouched. Such a highly reconfigurable structure not only provides exceptional convenience by minimizing the need for complex, redundant hardware, but also offers a significant advantage in rapidly adapting to varying trust levels across intermediate network nodes.

The measured HOM visibility of 0.476, mathematically supported by time-resolved models and polarization sweeps, alongside the verified QBERs across all modes, confirms that the EOM-prepared WCS channels achieve the necessary indistinguishability for reconfigurable QKD

operations. Furthermore, because the sideband offset is governed by the RF drive, the system's operating wavelength can be easily tuned by adjusting the center wavelength of the laser. This integrated wavelength tunability suggests that our proposed methodology is a highly promising approach for the development of scalable, re-

configurable quantum communication networks.

ACKNOWLEDGMENTS

This work was supported by an Agency for Defense Development grant funded by the Korean Government.

-
- [1] C. K. Hong, Z. Y. Ou, and L. Mandel, "Measurement of subpicosecond time intervals between two photons by interference," *Phys. Rev. Lett.* **59**, 2044–2046 (1987).
- [2] F. Bouchard, A. Sit, Y. Zhang, R. Fickler, F. M. Miatto, Y. Yao, F. Sciarrino, and E. Karimi, "Two-photon interference: the Hong–Ou–Mandel effect," *Rep. Prog. Phys.* **84**, 012402 (2021).
- [3] T. Legero, T. Wilk, A. Kuhn, and G. Rempe, "Time-resolved two-photon quantum interference," *Appl. Phys. B* **77**, 797–802 (2003).
- [4] Y.-S. Kim, O. Slattery, P. S. Kuo, and X. Tang, "Conditions for two-photon interference with coherent pulses," *Phys. Rev. A* **87**, 063843 (2013).
- [5] Y.-S. Kim, O. Slattery, P. S. Kuo, and X. Tang, "Two-photon interference with continuous-wave multi-mode coherent light," *Opt. Express* **22**, 3611–3620 (2014).
- [6] T. Ferreira da Silva, G. C. do Amaral, D. Vitoreti, G. P. Temporão, and J. P. von der Weid, "Spectral characterization of weak coherent state sources based on two-photon interference," *J. Opt. Soc. Am. B* **32**, 545–549 (2015).
- [7] E. Moschandreou, J. I. Garcia, B. J. Rollick, B. Qi, R. Pooser, and G. Siopsis, "Experimental study of Hong–Ou–Mandel interference using independent phase randomized weak coherent states," *J. Lightwave Technol.* **36**, 3752–3759 (2018).
- [8] H. Kim, D. Kim, J. Park, and H. S. Moon, "Hong–Ou–Mandel interference of two independent continuous-wave coherent photons," *Photon. Res.* **8**, 1491–1495 (2020).
- [9] H. Kim, O. Kwon, and H. S. Moon, "Time-resolved two-photon interference of weak coherent pulses," *Appl. Phys. Lett.* **118**, 244001 (2021).
- [10] F. Xu, X. Ma, Q. Zhang, H.-K. Lo, and J.-W. Pan, "Secure quantum key distribution with realistic devices," *Rev. Mod. Phys.* **92**, 025002 (2020).
- [11] H.-K. Lo, M. Curty, and B. Qi, "Measurement-device-independent quantum key distribution," *Phys. Rev. Lett.* **108**, 130503 (2012).
- [12] L. Lydersen *et al.*, "Hacking commercial quantum cryptography systems by tailored bright illumination," *Nat. Photonics* **4**, 686–689 (2010).
- [13] I. Gerhardt, Q. Liu, A. Lamas-Linares, J. Skaar, C. Kurtsiefer, and V. Makarov, "Full-field implementation of a perfect eavesdropper on a quantum cryptography system," *Nat. Commun.* **2**, 349 (2011).
- [14] A. Acín, N. Brunner, N. Gisin, S. Massar, S. Pironio, and V. Scarani, "Device-independent security of quantum cryptography against collective attacks," *Phys. Rev. Lett.* **98**, 230501 (2007).
- [15] A. Rubenok, J. A. Slater, P. Chan, I. Lucio-Martinez, and W. Tittel, "Real-world two-photon interference and proof-of-principle quantum key distribution immune to detector attacks," *Phys. Rev. Lett.* **111**, 130501 (2013).
- [16] Y. Liu *et al.*, "Experimental measurement-device-independent quantum key distribution," *Phys. Rev. Lett.* **111**, 130502 (2013).
- [17] Z. Tang, Z. Liao, F. Xu, B. Qi, L. Qian, and H.-K. Lo, "Experimental demonstration of polarization encoding measurement-device-independent quantum key distribution," *Phys. Rev. Lett.* **112**, 190503 (2014).
- [18] Y.-L. Tang *et al.*, "Measurement-device-independent quantum key distribution over untrustful metropolitan network," *Phys. Rev. X* **6**, 011024 (2016).
- [19] B. Qi, H.-K. Lo, C. C. W. Lim, G. Siopsis, E. A. Chittambar, R. Pooser, P. G. Evans, and W. Grice, "Free-space reconfigurable quantum key distribution network," in *2015 IEEE International Conference on Space Optical Systems and Applications (ICSOS)* (IEEE, 2015), arXiv:1510.04891.
- [20] G.-J. Fan-Yuan *et al.*, "Measurement-device-independent quantum key distribution for nonstandalone networks," *Photon. Res.* **9**, 1881–1891 (2021).
- [21] H. P. Lo and H. Takesue, "Precise tuning of single-photon frequency using an optical single sideband modulator," *Optica* **4**, 919–923 (2017).